Original Article

Feasibility of Proton Range Estimation with Prompt Gamma Imaging in Proton Therapy of Lung Cancer: Monte Carlo Study

Elham Rohollahpour, Hadi Taleshi Ahangari

Department of Medical Physics, School of Medicine, Semnan University of Medical Sciences, Semnan, Iran

Abstract

Context: Using prompt gamma (PG) ray is proposed as a promising solution for *in vivo* monitoring in proton therapy. Despite significant and diverse approaches explored over the past two decades, challenges still persist for more effective utilization. **Aims:** The feasibility of estimating proton range with PG imaging (PGI) as an online imaging guide in an anthropomorphic phantom with lung cancer was investigated through GATE/GEANT4 Monte Carlo simulation. **Setting and Design:** Once the GATE code was validated for use as a simulation tool, the gamma energy spectra of NURBS-based cardiac-torso (NCAT) and polymethyl methacrylate phantoms, representing heterogeneous and homogeneous phantoms respectively, were compared with the gamma emission lines known in nuclear interactions with tissue elements. A 5-mm radius spherical tumor in the lung region of an NCAT phantom, without any physiological or morphological changes, was simulated. **Subjects and Methods:** The proton pencil beam source was defined as a function of the tumor size to encompass the tumor volume. The longitudinal spatial correlation between the proton dose deposition and the distribution of detected PG rays by the multi-slit camera was assessed for proton range estimation. The simulations were conducted for both 10^8 and 10^9 protons. **Results:** The deviation between the proton range and the range estimated by PGI following proton beam irradiation to the center of the lung tumor was determined by evaluating the longitudinal profiles at the 80% fall-off point, measuring 1.9 mm for 10^9 protons and 4.5 mm for 10^8 protons. **Conclusions:** The accuracy of proton range estimation through PGI is greatly influenced by the number of incident protons and tissue characteristics. With 10^9 protons, it is feasible to utilize PGI as a real-time monitoring technique during proton therapy for lung cancer.

Keywords: Anthropomorphic phantom, lung cancer, Monte Carlo simulation, prompt gamma imaging, proton range estimation

Received on: 14-04-2024 **Review completed on:** 14-09-2024 **Accepted on:** 16-09-2024 **Published on:** 18-12-2024

Introduction

Cancer remains a significant contributor to morbidity and mortality in the modern era. Treatment options encompass radiation therapy, surgery, chemotherapy, and hormonal therapy. Radiation therapy can be delivered externally or internally.[1] Proton therapy, a form of external beam radiation therapy, utilizes proton particles in the treatment of lung cancer.[2] The distinct Bragg peak feature in the energy deposition curve of the proton beam sets this method apart from traditional radiotherapy. However, due to inherent range uncertainties,[3] precise estimation of range and local dose distribution is essential through *in vivo* monitoring to ensure treatment plan adherence and the protection of normal tissues and at-risk organs. Various techniques such as magnetic resonance imaging, ion acoustic tomography, interaction vertex imaging, positron emission tomography (PET), and prompt gamma imaging (PGI) are currently employed for *in vivo* verification of proton range to mitigate range uncertainties.[4,5] PET and PGI rely on detecting secondary particles resulting from the interaction of proton beams with matter. PG rays are emitted shortly after the inelastic interaction between a proton beam and the nucleus of a target atom. PGI was initially proposed by Stichelbaut and Jongen in 2003[6] and experimentally conducted by Min *et al*. in 2006[7] with the first patient undergoing PGI with dual scatter treatment in 2016 at the University of Protonen Therapie Dresden.[8] The real-time monitoring capability of PG rays, with their rapid diffusion following nuclear interactions, presents a notable advantage compared to PET imaging, which experiences delayed signals

Address for correspondence: Dr. Hadi Taleshi Ahangari, Department of Medical Physics, School of Medicine, Semnan University of Medical Sciences, Semnan, Iran.
E-mail: taleshi@semums.ac.ir

Access this article online

Quick Response Code:

Website: www.jmp.org.in

DOI: 10.4103/jmp.jmp_74_24

How to cite this article: Rohollahpour E, Ahangari HT. Feasibility of proton range estimation with prompt gamma imaging in proton therapy of lung cancer: Monte Carlo study. J Med Phys 2024;49:531-8.

and biological washout effects. Figure 1 illustrates the timescale of PG rays in comparison to gamma PET emission. In addition, PG beams offer a broad energy spectrum of approximately 15 MeV, derived from excited nucleus states and unique to each element, facilitating valuable insights into tissue composition and element density for spectral analysis.[9]

Exploring the utilization of PG can be categorized into two main groups. The first group includes slit cameras, prompt-gamma timing, peak integrals, prompt-gamma spectroscopy, and gamma-electron vertex imaging, which offer one-dimensional (1D) insights into PG distribution for verifying beam range. On the other hand, Compton cameras and PET provide three-dimensional (3D) reconstructions of deposited doses.[10] Currently, there are two detector designs for mapping the PG distribution position in imaging techniques: Passive (mechanical) collimation systems[11-13] such as slit cameras positioned perpendicularly to the beam direction, providing a 1D projection of the proton track, and active (electronic) collimation systems that utilize Compton kinematics to track the gamma source and prepare two-dimensional or 3D images.[14-16] The findings suggest that PGI serves as a dependable method for *in vivo* monitoring in proton therapy. Quantitative data validate the relationship between proton beam range and the distal edge of PG distribution in both homogeneous (water, polymethyl methacrylate [PMMA] phantom) and heterogeneous (DICOM-format phantom) targets.[14-16]

When calculating dose distributions with ions, addressing Bragg peak range uncertainty is crucial. Monte Carlo (MC) simulation, despite the limitations in the detailed examination of all the components contributing to range uncertainties such as converting Hounsfield units to the relative stopping power of protons, still helps to improve the accuracy of dose calculation in heterogeneous media and plays a significant role in commercial treatment planning systems to dose calculation instead of analytical calculation procedure.[17]

Past research has showcased the verification of proton beam range through the analysis of PG distributions in proton therapy's assessment using various imaging cameras in both homogeneous and heterogeneous targets, through simulations and experimental approaches. While research has validated the range for head and neck as well as prostate patients

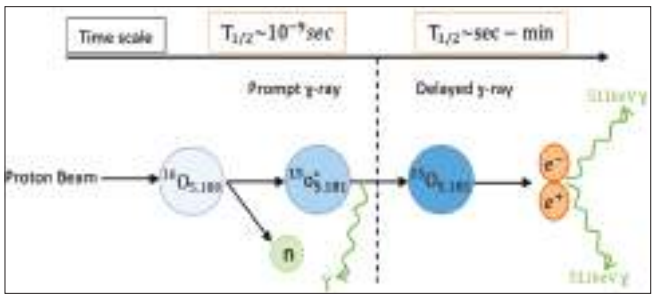

Figure 1: Time scale of prompt and positron emission tomography gamma-ray emissions

using PGI,[14-16] there is still a gap in comprehensive research for predicting the range in lung cancer with PGI. In this latest study, the feasibility of estimating proton range was explored by assessing PG distributions with the multi-slit camera, as detailed by Min *et al*.,[18] for *in vivo* monitoring during proton therapy for lung cancer on a NURBS-based cardiac-torso (NCAT) anthropomorphic phantom using MC simulations.

The study not only delves into the technical aspects of MC simulations and proton range assessment but also highlights the potential impact of PGI in improving the accuracy of proton therapy for lung cancer. By exploring innovative methods such as the multi-slit camera and advanced detection systems, the research paves the way for more effective and precise monitoring of proton beam ranges during treatment, ultimately enhancing patient outcomes in lung cancer therapy.

Subjects and Methods

Monte Carlo simulations

MC simulation was conducted to model proton beam radiation and a sophisticated collimator/detector camera using GATE v8, based on GEANT4 (v10.3.3), to facilitate the study of PGI in proton therapy. The chosen physics list, QGSP_BIC_HP_EMY, accounts for electromagnetic and hadronic processes and demonstrates good alignment with PG measurements.[19,20] The simulation utilized the Option 3 electromagnetic standard package parameters, employing the G4UHadronElasticProcess in combination with the G4HadronElastic model for elastic hadronic interactions and the Binary Cascade model for inelastic interactions. By setting minimum kinetic energy thresholds for particles, only those with sufficient momentum could escape the phantom. Range cuts were established for all particles, while Variance Reduction Techniques were not utilized.

Validation of GATE code

The validation of the GATE code involved comparing the range produced by a simulated incident proton beam in a cubic water phantom measuring 400 mm × 400 mm × 400 mm across five clinical energies with the known proton beam range data from the NIST library. This library contains range and stopping power tables based on the continuous-slowing-down approximation in various materials. The study utilized optimized source parameters recommended by Grevillot *et al*., where the position of the Bragg peak and range were determined based on the dose distribution in the Bragg curve. In this study, simulations of the proton range and proton pencil beam features at different depths and energies between 60 and 250 MeV have been assessed against reference measurements in water and PMMA.[21] Table 1 describes the properties of the pencil beam source. The position of the Bragg peak and the range are determined as the maximum dose point and 80% of the maximum dose point in the Bragg curve as the distal edge, respectively.[3]

Simulation of prompt gamma imaging

Case study

The four-dimensional-anthropomorphic phantom NCAT, created by Segars and Tsui,[22] was utilized for this study. The lung region of the phantom was defined as a 256 mm × 256 mm × 300 mm dosimetry matrix with a voxel size of 1 mm × 1 mm × 1 mm, without any physiological or morphological alterations. Various tissue-equivalent materials from the Geant4 NIST database were assigned to the NCAT phantom. To simulate lung cancer, a spherical tumor with a 5 mm radius, based on data from the International Association for the Study of Lung Cancer, was positioned at the anterior of the right lung in the phantom.

Drawing from the work of Sterpin *et al*.,[23] the human body's tissues were assumed to be composed primarily of nuclei such as ^{1}H, ^{12}C, ^{14}N, and ^{16}O. The proton flow was influenced by the elastic proton–proton interaction, with a ^{1}H weight fraction for most tissues matching the gamma spectrum at 10% (according to ICRU44) without impacting the gamma spectrum itself.[24] To validate the MC simulations, the gamma-ray spectrum fluence was calculated for both a PMMA phantom and the NCAT phantom of the same size, using gamma emission cross-section data reported by Kozlovsky *et al*.[25] within a 2–8 MeV energy window. A total of 10^8 protons with an energy of 60 MeV and a lateral full-width-at-half-maximum of 9 mm, representative of current PBS systems,[26] were irradiated onto both phantoms.

System set-up

Distribution profiles and data acquisition

Recent investigations have identified two key challenges in capturing the PG distribution: The isotropic emission of PGs following proton beam collisions with target nuclei at energies above 4 MeV, and the significant generation of neutrons resulting from proton-induced nuclear interactions. Min *et al*.,[18] successfully addressed these challenges by utilizing a collimator-based system positioned at 90° to the proton beam, coupled with a scintillation array and a multichannel data acquisition system. This setup enabled the verification of the correlation between detection profiles and the proton range. Consequently, in this study, the distribution of PGs at 90° through the lateral collimator was detected.

Camera system

The collimation imaging system employed for gamma imaging utilizes multi-slit collimators to capture PG rays emitted perpendicular to the proton beam path. Previous MC simulations determined the optimal thickness of the slit and septal to be 2 mm,[18] resulting in a slit pitch of 4 mm (pitch = slit + septal). The system comprises four rows of multi-slit collimators and 64 CsI (Tl) scintillator arrays located behind the slits. The configuration and structure of the detection system are outlined in Table 2 and Figure 2, respectively, with the length of the slit set at 100 mm to limit unwanted radiation penetration through the septal to below 10%.[27] Figure 2 depicts the geometry of the multi-slit detection system from both a top view and a side view.

Table 1: Properties of proton pencil beam

Energy beam	60, 100, 150, 200, 250 MeV
Sigma energy (σ_E)	0 MeV
Spot size ($\sigma_{x,y}$)	3 mm
Divergence	3 mrad

Table 2: Characteristics of the structure of multi-slit detection system

Structure	Material	Density (g/cm^3)	Thickness (mm)	Width (mm)	Height (mm)
Septal	Tungsten	19.3	2	100	100
Crystal array	CsI (Tl) scintillator	4.51	3	30	100

PG rays distribution was examined at varying distances (100, 140, 180, 220, and 260 mm) between a cubic PMMA phantom (size: 256 mm × 256 mm × 300 mm) and the camera system surface following the irradiation of a 60 MeV proton beam directed at the center of the phantom along the y-axis.

Postsimulation data analysis

Postsimulation data analysis involved determining the 1D spatial correlation by calculating the difference between the proton beam range (R_{Proton}) – defined as the point with an 80% distal dose decrease along the beam path – and the PG rays range (R_{PG}), assessed through sigmoid curve fitting applied to the PG rays distribution profiles to identify the 80% distal fall-off.[18]

$$Y = \frac{A_1 - A_2}{1 + e^{(x - x_0)/dx}} + A_2$$

x is the distance traveled by the proton beam in the phantom. The sigmoid curve function utilized in this analysis involved fitting parameters A_1, A_2, x_0, and dx, where x_0 indicated the inflection point defining RPG, dx represented the width between data points, and the minimum and maximum value of PG rays distribution was determined by parameter A_1 and A_2.

Proton rang estimation in the case study

To proton range estimation, we used the ICRU63 report that states 98% of the tumor volume receives at least 98% of the prescribed dose. In other words, D98 ≥98% was considered in this study. To achieve this, a new proton beam source was developed to generate Gaussian single pencil beams with energy spread and spatial beam spread distributions proportional to tumor size. These beams were irradiated at three estimated energies to produce dose profiles along the radiation direction.

In conducting the simulation, 10^8 representative protons, equivalent to the most distal pencil beam in a typical treatment plan,[28] and at least 10^9 protons to mitigate statistical effects (because proton beam range should be smaller than the

range uncertainties) were directed toward the lung tumor along the y-axis. Subsequently, the PG rays distribution profile was obtained by positioning the camera system with a 2–8 MeV window to the right side of the NCAT phantom.

Results

Validation of GATE code

Validation of the GATE code was performed by examining the proton depth-dose profiles in a water phantom across 5 clinical energies using the QGSP_BIC_HP_EMY physics list. Figure 3 depicts the $R_{80\%}$ difference between the results obtained from the GATE code and the NIST database, while Table 3 presents the numerical values of the relative percentage difference in the $R_{80\%}$ of the maximum dose between R_{GATE} and R_{NIST} across the 5 clinical energies.

The statistical analysis revealed a high level of agreement between R_{GATE} and R_{NIST}, with a sigma value of 0.997, indicating no significant difference, confirming the validation of the simulation code for this study, consistent with previous research.[29] As a result, the simulation code was deemed suitable for utilization in this study.

Gamma energy spectrum

Figure 4 displays the energy spectrum fluence of gamma rays emitted from both the NCAT and PMMA phantom following the delivery of a 60 MeV proton beam within a 2–8 MeV energy window. In addition, Table 4 presents the cross-section data of gamma emission lines resulting from nuclear interactions between protons and ^{12}C, ^{14}N, and ^{16}O targets spanning energies from 2 to 8 MeV.

By comparing the emitted gamma spectrum from both phantoms with the cross-section data provided in Table 1, peak intensities at energies of 2.31, 3.8, 4.44, 5.27, and 6.13 MeV were observed, originating from the interaction of protons with nuclei of tissue elements such as ^{12}C, ^{14}N, and ^{16}O.

Proton range estimation

The study focused on estimating the range value by analyzing the spatial correlation between PG ray distribution and proton deposit dose. R_{PG} was defined as the inflection point position in the sigmoid curve fitted to the PG rays distribution profile and compared with R_{Proton} in the 80% distal fall-off. The accuracy of range estimation and goodness-of-fit statistics were evaluated using the R^2 index ($R^2 \geq 0.99$), representing the correlation between response values and predicted response values.

Distance of camera system

Due to the simulation output was in phase space format, the distribution of photons can be obtained at any depth. Figure 5 illustrates the longitudinal PG rays distribution emitted from the cubic PMMA phantom at varying distances from 100 mm to

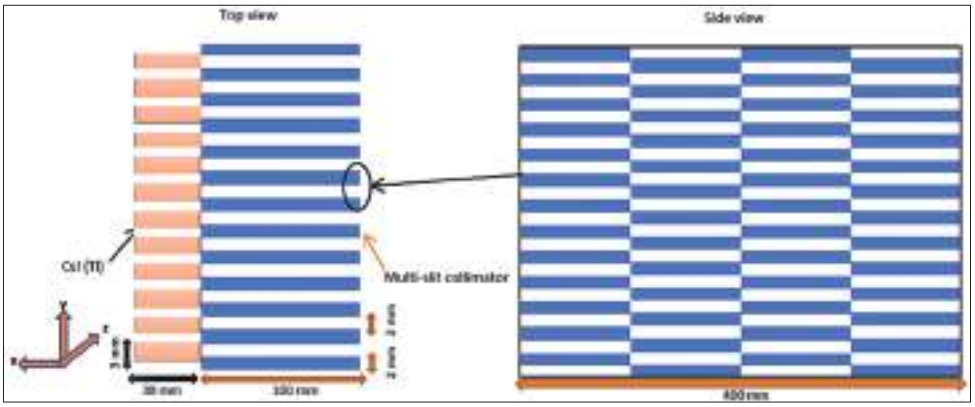

Figure 2: The multi-slit detection system. The Region of Interest is shown in side view on the right

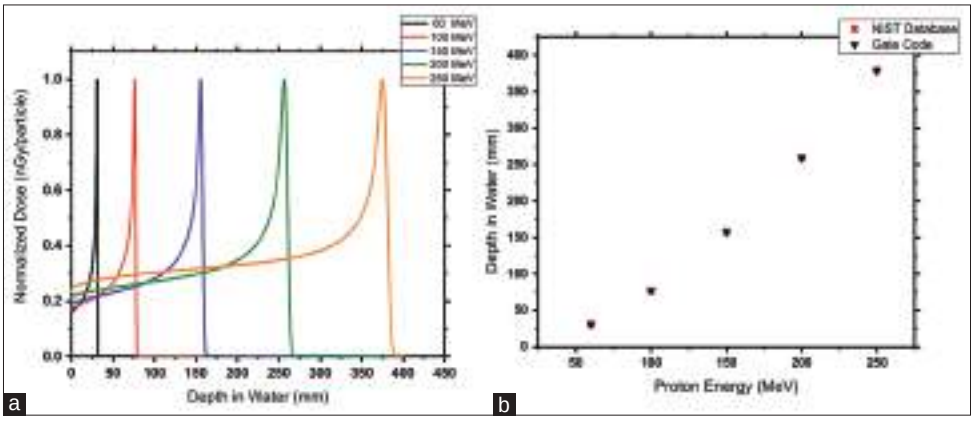

Figure 3: (a) Proton depth dose profile, normalized by the maximum dose, (b) $R_{80\%}$ differences in GATE code and NIST database

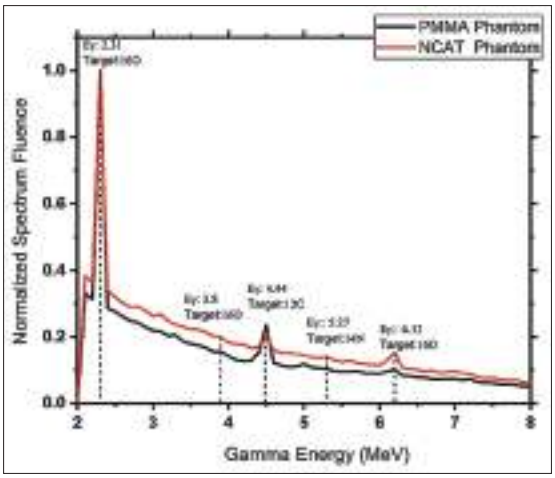

Figure 4: Gamma spectrum fluence emitted by irradiated 60 MeV proton beam to NURBS-based cardiac-torso and polymethyl methacrylate phantom. NCAT = NURBS-based cardiac-torso, PMMA = Polymethyl methacrylate

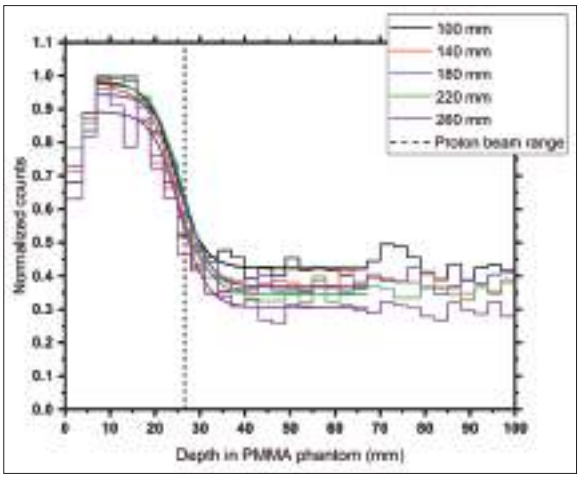

Figure 5: R_{PG} at different distances from polymethyl methacrylate phantom surface to the detection system surface. PMMA = Polymethyl methacrylate

260 mm in 40 mm intervals from the phantom to the camera system surface. The beam energy considered was 60 MeV with a range of 26.6 mm, and a total of 10^9 protons were used. Table 5 showcases the difference between R_{proton} and R_{PG} at different distances.

The results indicated that increasing the distance between the detection system and the PMMA phantom did not significantly affect the range estimated by PGI. However, a distance of 220 mm was selected due to the minimal difference between R_{proton} and R_{PG}.

Proton range estimation with prompt gamma imaging in lung cancer

The feasibility of using PGI for proton range estimation in lung cancer was investigated by defining a new source aimed at achieving 98% coverage of tumor volume by adjusting beam properties based on tumor size. Figure 6 displays longitudinal profiles of proton dose deposition at three estimated energies, showing the confirmation of the Brag Peak (BP) position in a 77 MeV proton energy with a range of 100 mm positioned at the center of the lung tumor. It is crucial to mention that the estimated range includes the first 50 mm within the air space of our phantom dosimetry matrix. The beam penetrates the body beyond this point, resulting in an actual range within the body that is <100 mm. This description is shown in Figure 7.

Table 6 showcases the difference between the R_{NIST} value of the 77 MeV beam in water and the estimation of the water equivalent thickness of the Bragg peak position and distal fall-off position of the 80% of the peak (R_{PG}) value in the NCAT phantom from PG simulation [Figure 8].

Furthermore, Figure 9 depicts the longitudinal PG rays distribution and proton dose deposit profiles along the irradiated proton beam path to the lung tumor with 10^8 and 10^9 protons and 77 MeV energy.

In summary, we have determined the PG distribution profile for the postproton beam irradiation of the lung region of the

Table 3: Characteristic beam range parameter R_{GATE} in water and comparison with R_{NIST} and along with relative percentage difference of 80% of the maximum dose

Energy (MeV)	R_{GATE} (mm)	R_{NIST} (mm)	Difference (%)
60	30.9	30.9	0
100	77.1	77.2	0.13
150	157.5	157.7	0.127
200	259.1	259.6	0.193
250	378.7	379.4	0.185

Table 4: Available experimental cross-section data of gamma emission lines from nuclear interactions with ^{12}C, ^{14}N, and ^{16}O targets at energies of 2–8 MeV[25]

Target	Emitted Particle	E_γ (MeV)	Transition
^{12}C	^{12}C	4.44	$^{12}C_{4.44}{}^{*}\rightarrow{}^{12}C_{g.s.}$
^{14}N	^{14}N	2.133	$^{14}N_{2.13}{}^{*}\rightarrow{}^{14}N_{g.s.}$
	^{15}N	5.27	$^{12}C_{5.27}\rightarrow{}^{15}N_{5.27}$
^{16}O	^{16}O	6.13	$^{16}O_{6.13}{}^{*}\rightarrow{}^{16}O_{g.s.}$
		6.92	$^{16}O_{6.916}\rightarrow{}^{16}O_{6.917}$
	^{14}N	2.31	$^{16}O_{2.31}\rightarrow{}^{14}N_{2.31}$
	^{15}N	5.27	$^{16}O_{5.269}\rightarrow{}^{15}N_{5.27}$
	^{13}C	3.8	$^{16}O_{3.853}\rightarrow{}^{13}C_{3.854}$

g.s.=Ground state, * = excited state

NCAT phantom with 10^8 and 10^9 protons by MC simulation of a multi-slit detection system. It is found that the estimated R_{PG} approaches R_{Proton} as the number of protons increases in table 7.

The study suggested the potential of using PGI as an *in vivo* monitoring method in proton therapy for lung cancer, particularly when a sufficient number of protons is utilized.

Discussion

In the present study, we attempted to investigate the feasibility of using PGI with a multi-slit camera system to estimate

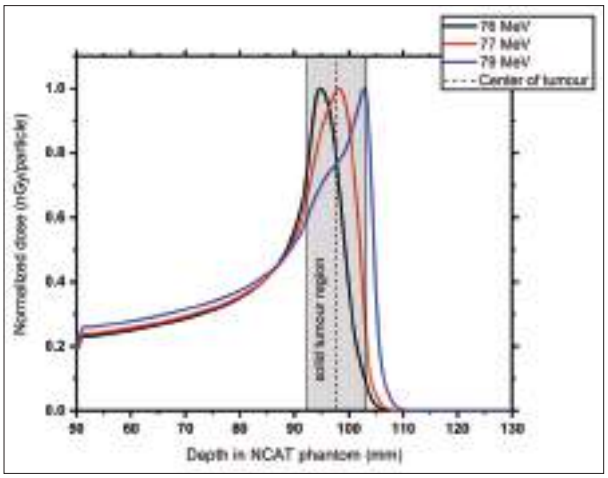

Figure 6: Longitudinal profiles of proton dose deposition in 3 estimated energies, normalized by maximum dose. NCAT = NURBS-based cardiac-torso

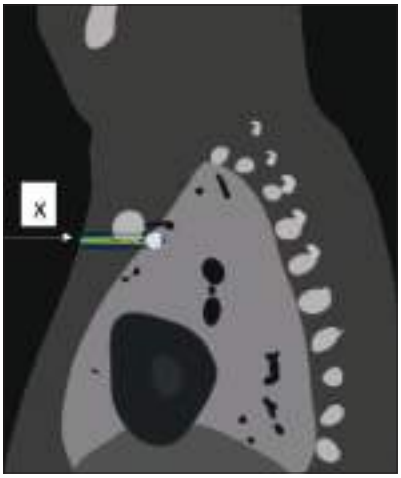

Figure 7: NURBS-based cardiac-torso phantom cross-section for estimating proton range in the lung: The X distance in airspace should be considered

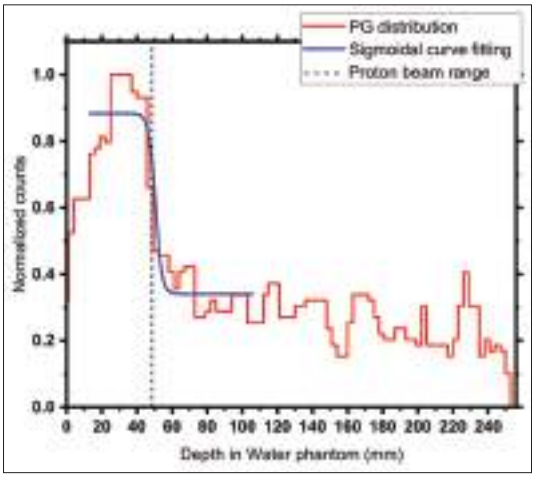

Figure 8: Longitudinal prompt gamma ray's distribution and proton beam range with 10^8 protons in water phantom. PG = Prompt gamma

proton beam range for *in vivo* monitoring during lung cancer treatment by MC simulation. Many studies showed that PG

Table 5: The difference between proton beam range and the prompt gamma distribution range in different distance from phantom surface to camera system surface

Distance from phantom surface to camera system surface (mm)	R_{PG} (mm)	$\Delta (R_{Proton} - R_{PG})$ (mm)
100	24	2.6
140	24.1	2.5
180	25.4	1.2
220	25.5	1.1
260	25	1.6

Table 6: The difference between proton beam range in water and the prompt gamma distribution range in the NURBS-based cardiac-torso T phantom

Proton energy (MeV)	R_{PG} (mm)	R_{NIST} (mm)	$\Delta (R_{PG} - R_{NIST})$ (mm)
77	50.4	48.6	1.8

Table 7: Prompt gamma-ray range and difference from proton beam range for the different number of delivered protons

Number of delivered protons	R_{PG} (mm)	$\Delta (R_{Proton} - R_{PG})$ (mm)
10^8	95.5	4.5
10^9	98.1	1.9

rays emitted by the inelastic interaction of a target nucleus and incident protons are strongly related to the elemental compositions of the target.[30-33] Simulations were performed on anthropomorphic NCAT phantom without physiologic/morphological changes. To study lung cancer as one of the most common types of cancer in the world, a spherical tumor with a radius of 5 mm was created in a specific section of the lung region in Phantom. The PMMA phantom was used as a homogeneous phantom in several studies,[7,19,24] verification of the MC simulations was determined by comparing the gamma spectrum obtained from both phantoms and the cross-section data of gamma emission lines, it was proved that the highest gamma spectrum peaks were at the energies of 2.31, 3.8, 4.44, 5.27, and 6.13 MeV energies, which belong to the gammas emitted from the interaction of protons with the nuclei of ^{12}C, ^{14}N, and ^{16}O tissue elements. PGI system with a multi-slit collimator and CsI (Tl) scintillator arrays was simulated.[7,28,34] Evaluation of the consequence of changing the distance between the phantom surface and detection camera surface on the range estimation accuracy showed that changing the distance from 100 to 260 mm will not significantly affect the proton beam range estimation results. The longitudinal spatial correlation between the PG rays distribution and the proton dose deposition profiles was analyzed with sigmoid curve fitting. For 10^9 protons, the difference in estimated range and proton beam range was 1.9 mm, which is approximately

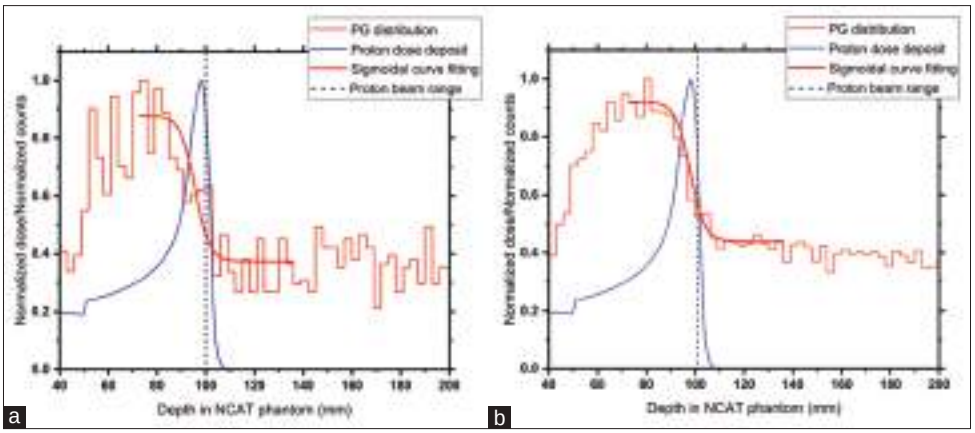

Figure 9: Longitudinal prompt gamma ray's distribution and proton dose deposit profiles with (a) 108, (b) 109 protons. PG = Prompt gamma

1.9% of the proton beam range and smaller than the range uncertainties and typical safety margin. According to the PG distribution diagram in Figure 9, the highest PG distribution is in the path of the proton beam entering the body until it reaches the lung wall, and after that, despite the maximum dose deposit to the lung tumor, the intensity of the PG distribution is greatly reduced in this region, which indicates that the PG longitudinal distribution variation is sensitive and intensely depends on the elemental composition and the medium density in the heterogeneous phantoms, as also observed in previous work.[31-33,35] Results generally like the last studies show that the range estimation is dependent on the number of protons.[32,36,37] One of the goals of this work was to investigate and evaluate the relationship between PG ray distribution and proton dose deposition using MC simulation calculations with minimal proton tracking. The comprehensive investigation conducted in this study demonstrates the potential utility of PGI for accurate proton range estimation in lung cancer treatment scenarios. By employing MC simulations and advanced detection systems, such as multi-slit collimators and CsI (Tl) scintillator arrays, the study successfully assessed the spatial correlation between PG ray distributions and proton dose depositions. This approach offers promising prospects for real-time monitoring of proton beam ranges during treatment.

Conclusions

The findings highlight the importance of elemental compositions and tissue densities in influencing PG distributions, emphasizing the need for precise modeling and analysis in heterogeneous phantom scenarios. Through rigorous analysis and validation, the study showcased the effectiveness of PGI in estimating proton ranges with a high degree of accuracy, as evidenced by the minimal differences observed between estimated and actual proton ranges.

Looking ahead, future research endeavors will focus on expanding the scope of PGI applications to encompass varying tumor sizes and configurations. In addition, efforts will be directed toward enhancing imaging capabilities to provide 3D insights into PG distribution. By advancing the capabilities of PGI technology and refining the analytical methodologies, this study sets the stage for transformative progress in proton therapy for lung cancer treatment. The integration of PGI as an *in vivo* monitoring tool holds great promise for optimizing treatment outcomes and ensuring the efficacy of proton therapy strategies.

Acknowledgment

This article is an excerpt from the thesis research project approved at Semnan University of Medical Sciences with the code of ethics IR.SEMUMS.REC.1400.243. In this way, the authors express their gratitude and appreciation for the financial support of the research assistants of university.

Financial support and sponsorship

This work was supported by Semnan University of Medical Sciences.

Conflicts of interest

There are no conflicts of interest.

References

1. Sadeghi M, Enferadi M, Shirazi A. External and internal radiation therapy: Past and future directions. J Cancer Res Ther 2010;6:239-48.
2. Rana S, Simpson H, Larson G, Zheng Y. Dosimetric impact of number of treatment fields in uniform scanning proton therapy planning of lung cancer. J Med Phys 2014;39:212-8.
3. Paganetti H. Range uncertainties in proton therapy and the role of Monte Carlo simulations. Phys Med Biol 2012;57:R99-117.
4. Knopf AC, Lomax A. *In vivo* proton range verification: A review. Phys Med Biol 2013;58:R131-60.
5. Tu WY, Zhang ZY, Jun Z, Xu XL, Ding JP, Su JH, *et al.* Positron imaging for verification of irradiation field during radiotherapy. J Cancer Res Ther 2018;14:S416-20.
6. Stichelbaut F, Jongen Y, editors. Verification of the Proton beam Position in the Patient by the Detection of Prompt Gamma-Rays Emission. 39th Meeting of the Particle Therapy Co-Operative Group; 2003.
7. Min CH, Kim CH, Youn MY, Kim JW. Prompt gamma measurements for locating the dose falloff region in the proton therapy. Appl Phys Lett 2006;89:183517.
8. Richter C, Pausch G, Barczyk S, Priegnitz M, Keitz I, Thiele J, *et al.* First clinical application of a prompt gamma based *in vivo* proton range verification system. Radiother Oncol 2016;118:232-7.
9. Mackin D, Peterson S, Beddar S, Polf J. Evaluation of a stochastic reconstruction algorithm for use in Compton camera imaging and

beam range verification from secondary gamma emission during proton therapy. Phys Med Biol 2012;57:3537-53.
10. Wrońska A. Prompt gamma imaging in proton therapy-status, challenges and developments. Phys Conf Ser 2020;1561:012021.
11. Kim JW. Pinhole camera measurements of prompt gamma-rays for detection of beam range variation in proton therapy. J Korean Phys Soc 2009;55:1673-6.
12. Smeets J, Roellinghoff F, Prieels D, Stichelbaut F, Benilov A, Busca P, *et al.* Prompt gamma imaging with a slit camera for real-time range control in proton therapy. Phys Med Biol 2012;57:3371-405.
13. Bom V, Joulaeizadeh L, Beekman F. Real-time prompt γ monitoring in spot-scanning proton therapy using imaging through a knife-edge-shaped slit. Phys Med Biol 2012;57:297-308.
14. Kormoll T, Fiedler F, Schöne S, Wüstemann J, Zuber K, Enghardt W. A Compton imager for *in-vivo* dosimetry of proton beams – A design study. Nucl Instrum Methods Phys Res A 2011;626:114-9.
15. Peterson SW, Robertson D, Polf J. Optimizing a three-stage Compton camera for measuring prompt gamma rays emitted during proton radiotherapy. Phys Med Biol 2010;55:6841-56.
16. Polf JC, Avery S, Mackin DS, Beddar S. Imaging of prompt gamma rays emitted during delivery of clinical proton beams with a Compton camera: Feasibility studies for range verification. Phys Med Biol 2015;60:7085-99.
17. Kim DH, Cho S, Jo K, Shin E, Hong CS, Han Y, *et al.* Proton range verification in inhomogeneous tissue: Treatment planning system versus measurement versus Monte Carlo simulation. PLoS One 2018;13:e0193904.
18. Min CH, Lee HR, Kim CH, Lee SB. Development of array-type prompt gamma measurement system for *in vivo* range verification in proton therapy. Med Phys 2012;39:2100-7.
19. Robert C, Dedes G, Battistoni G, Böhlen TT, Buvat I, Cerutti F, *et al.* Distributions of secondary particles in proton and carbon-ion therapy: A comparison between GATE/Geant4 and FLUKA Monte Carlo codes. Phys Med Biol 2013;58:2879-99.
20. Huisman BF, Létang JM, Testa É, Sarrut D. Accelerated prompt gamma estimation for clinical proton therapy simulations. Phys Med Biol 2016;61:7725-43.
21. Grevillot L, Frisson T, Zahra N, Bertrand D, Stichelbaut F, Freud N, *et al*. Optimization of GEANT4 settings for proton pencil beam scanning simulations using GATE. Nucl Instrum Methods Phys Res B 2010;268:3295-305.
22. Segars WP. Development of a new dynamic NURBS-based cardiac-torso (NCAT) phantom. PhD Thesis, The University of North Carolina at Chapel Hill ProQuest Dissertations and Theses 2001. 3007884.
23. Sterpin E, Sorriaux J, Vynckier S. Extension of PENELOPE to protons: Simulation of nuclear reactions and benchmark with Geant4. Med Phys 2013;40:111705.
24. Sterpin E, Janssens G, Smeets J, Vander Stappen F, Prieels D, Priegnitz M, *et al.* Analytical computation of prompt gamma ray emission and detection for proton range verification. Phys Med Biol 2015;60:4915-46.
25. Kozlovsky B, Murphy RJ, Ramaty R. Nuclear deexcitation gamma-ray lines from accelerated particle interactions. The Astrophysi J Suppl Ser 2002;141:523.
26. Parodi K, Mairani A, Brons S, Hasch BG, Sommerer F, Naumann J, *et al.* Monte Carlo simulations to support start-up and treatment planning of scanned proton and carbon ion therapy at a synchrotron-based facility. Phys Med Biol 2012;57:3759-84.
27. Cherry SR, Sorenson JA, Phelps ME. Physics in Nuclear Medicine e-Book. Philadelphia : Elsevier Health Sciences; 2012.
28. Smeets J, Roellinghoff F, Janssens G, Perali I, Celani A, Fiorini C, *et al.* Experimental comparison of knife-edge and multi-parallel slit collimators for prompt gamma imaging of proton pencil beams. Front Oncol 2016;6:156.
29. Zarifi S, Ahangari HT, Jia SB, Tajik-Mansoury MA. Validation of GATE Monte Carlo code for simulation of proton therapy using National Institute of Standards and Technology library data. J Radiother Pract 2019;18:38-45.
30. Verburg JM, Shih HA, Seco J. Simulation of prompt gamma-ray emission during proton radiotherapy. Phys Med Biol 2012;57:5459-72.
31. Janssens G, Smeets J, Vander Stappen F, Prieels D, Clementel E, Hotoiu EL, *et al.* Sensitivity study of prompt gamma imaging of scanned beam proton therapy in heterogeneous anatomies. Radiother Oncol 2016;118:562-7.
32. Priegnitz M, Helmbrecht S, Janssens G, Perali I, Smeets J, Vander Stappen F, *et al.* Measurement of prompt gamma profiles in inhomogeneous targets with a knife-edge slit camera during proton irradiation. Phys Med Biol 2015;60:4849-71.
33. Zarifi M, Guatelli S, Bolst D, Hutton B, Rosenfeld A, Qi Y. Characterization of prompt gamma-ray emission with respect to the Bragg peak for proton beam range verification: A Monte Carlo study. Phys Med 2017;33:197-206.
34. Park JH, Kim SH, Ku Y, Lee HS, Kim YS, Kim CH, *et al.* Correction of prompt gamma distribution for improving accuracy of beam range determination in inhomogeneous phantom. Prog Med Phys 2017;28:207-17.
35. Priegnitz M, Helmbrecht S, Janssens G, Perali I, Smeets J, Vander Stappen F, *et al.* Detection of mixed-range proton pencil beams with a prompt gamma slit camera. Phys Med Biol 2016;61:855-71.
36. Park JH, Kim SH, Ku Y, Kim CH, Lee HR, Jeong JH, *et al.* Multi-slit prompt-gamma camera for locating of distal dose falloff in proton therapy. Nucl Eng Technol2019;51:1406-16.
37. Pinto M, Dauvergne D, Freud N, Krimmer J, Letang JM, Ray C, *et al.* Design optimisation of a TOF-based collimated camera prototype for online hadrontherapy monitoring. Phys Med Biol 2014;59:7653-74.